JOURNAL OF THERMOPHYSICS AND HEAT TRANSFER
Vol. 9, No. 3, July–September 1995

Blunt Body Rarefied Wakes for Earth Entry

Virendra K. Dogra*
Science and Technology Corporation, Hampton, Virginia 23666
James N. Moss† and Richard G. Wilmoth‡
NASA Langley Research Center, Hampton, Virginia 23681-0001
and
Jeff C. Taylor§ and H. A. Hassan¶
North Carolina State University, Raleigh, North Carolina 27695

Direct simulation Monte Carlo (DSMC) and Navier–Stokes axisymmetric calculations are presented for hypersonic low-density flow about a 70-deg blunt cone afterbody configuration. The flow conditions simulated are those experienced by a space vehicle for an altitude range of 105–75 km during Earth entry. The entry velocity considered is 7 km/s. A steady vortex is predicted in the near wake for 75 and 85 km altitudes by both calculations. The flow remains attached for 95 and 105 km altitudes. Comparisons of DSMC and Navier–Stokes calculations for the wake flowfield become less and less favorable with increasing altitude. Comparisons of surface quantities show reasonable agreement between DSMC and Navier–Stokes calculations along the forebody. However, the surface quantities along the afterbody calculated from DSMC and Navier–Stokes calculations differ significantly at the higher altitudes.

Nomenclature

A = base area of cone, $\pi d^2/4$
C_D = drag coefficient, $2D/\rho_\infty V_\infty^2 A$
C_f = skin friction coefficient, $2\tau_w/\rho_\infty V_\infty^2$
C_H = heat transfer coefficient, $2q/\rho_\infty V_\infty^3$
C_i = mass fraction of species i
C_p = pressure coefficient, $2p/\rho_\infty V_\infty^2$
D = drag
d = base diameter, 2.65 m
d_{ref} = molecular diameter at reference temperature
Kn = Knudsen number, λ/d
M = Mach number
$\mathcal{M}$ = molecular weight of air
N = atomic nitrogen
N_2 = molecular nitrogen
$\mathcal{N}$ = Avogadro's number, 6.02252×10^{26} particles/kg − mole
O = atomic oxygen
O_2 = molecular oxygen
p = pressure
q = heat flux
R_b = cone base radius
R_c = corner radius
Re = Reynolds number, $\rho V d/\mu$
Re_2 = total Reynolds number, $Re_\infty(\mu_\infty/\mu_0)$
R_n = cone nose radius
$\mathcal{R}$ = universal gas constant, 8.3143 J/mol − K
S = speed ratio, $V\sqrt{\mathcal{M}/2\mathcal{R}T}$
s = distance along the body surface measured from the stagnation point
$\bar{s}$ = temperature exponent of the coefficient of viscosity
T = thermodynamic temperature
T_r = rotational temperature
T_t = translational temperature
T_v = vibrational temperature
T_w = surface temperature
u = axial velocity
V = velocity
v = radial velocity
X_i = mole fraction of species i
x = axial distance from stagnation point measured along symmetry axis
x_a = location of rear stagnation point
x_b = location of wake stagnation point
y = radial distance from symmetry axis
Γ = gamma function
λ = mean free path
μ = dynamic viscosity
ρ = density
σ = collision cross section
τ = shear stress

Subscripts
ref = reference value
stag = stagnation point
w = surface values
∞ = freestream values

Presented as Paper 94-2016 at the AIAA/ASME 6th Joint Thermophysics and Heat Transfer Conference, Colorado Springs, CO, June 20–23, 1994; received Sept. 12, 1994; revision received Jan. 30, 1995; accepted for publication Jan. 30, 1995. This paper is declared a work of the U.S. Government and is not subject to copyright protection in the United States.

*Research Engineer, Aerospace Group. Associate Fellow AIAA.
†Research Engineer, Aerothermodynamics Branch. Fellow AIAA.
‡Research Engineer, Aerothermodynamics Branch. Senior Member AIAA.
§Research Assistant, Mechanical and Aerospace Engineering. Student Member AIAA.
¶Professor, Mechanical and Aerospace Engineering. Associate Fellow AIAA.

Introduction

FROM an aerothermodynamic standpoint, knowledge of blunt body wake structure is very important for the design of planetary probes and aerobrakes. Precise determination of wake closure is a critical issue for aerobrakes because the low lift-to-drag ratio aeroshell designs impose constraints on payload configuration. The payload must fit into the wake cone to minimize afterbody heating since a heating spike is generally associated with wake reattachment. Because of the complicated nature of wake flows a perception exists[1] that the wake aerothermodynamics cannot be predicted accurately. The fundamental issues concerning such flows are the effects of rarefaction and thermochemical nonequilibrium on the wake

structure and the extent to which the continuum modeling is valid to simulate these flows. Recent, computational investigations[2-12] of blunt body wake structure have looked into some of these issues to isolate critical features of the blunt body wake structure.

Generally, two methods are used to simulate blunt body wake flows at high altitudes. First is the continuum approach in which a set of model equations is solved numerically, and normally this set is the Navier–Stokes equations. The Navier–Stokes modeling becomes inadequate for large local Knudsen numbers such as those occurring when the relatively high-density forebody flow expands into the wake. The second method is of a molecular nature where a direct physical simulation is done by following the motion and interaction of modeled molecules. This method is equally valid at low and high local Knudsen numbers and, therefore, it is more appropriate to simulate the wake flows with the molecular method under rarefied conditions. In the present study, computational codes representative of both methods are used for an altitude range of 105–75 km to simulate hypersonic wake flows about a 70-deg sphere cone with a base radius of 1.325 m, a nose radius of 0.6625 m, a shoulder radius of 0.06625 m, and a afterbody configuration. The molecular simulations are achieved with Bird's[13-15] direct simulation Monte Carlo (DSMC) method whereas the continuum simulations are performed using the Navier–Stokes code developed by Olynick and Hassan.[16,17]

The objectives of this article are to provide an improved understanding of the effects of rarefaction and thermochemical nonequilibrium on blunt body wake structure at flight conditions and to identify flow conditions where Navier–Stokes calculations with slip boundary conditions become deficient.

Computational Method and Boundary Conditions

Both the molecular and continuum methods used in the present calculations are briefly described next.

Molecular Method

The DSMC method[13-15] is used for the present calculations. The method and requirements for application of DSMC have been presented in previous publications[18,19] and are not repeated here.

The computational domain used for the calculations is large enough to capture most of the body disturbance at the upstream and side boundaries. Thus, freestream conditions are specified at these boundaries. The flow at the downstream outflow boundary is supersonic and vacuum conditions are specified.

The flowfield was divided into several regions and a fine grid resolution was used for cells along the body and in the wake. This was achieved by conducting several grid refinements for each flow condition. The cell dimension normal to the body surface in the forebody and wake was of the order of half of the local mean free path except for the lowest altitude case (75 km). For the lowest altitude case the cell dimension normal to the body surface in the forebody and wake regions was the order of the local mean free path. Steady state was assumed when the number of simulated molecules in each region achieved a fixed value within fluctuations of 1%. The average number of simulated molecules in a cell was 20 at steady state. The final results were obtained through a time-averaged solution over a large number of time steps.

The molecular collisions are simulated by the variable hard sphere (VHS) molecular model. This model employs the simple hard-sphere angular-scattering law so that all directions are equally possible for the postcollision velocity in the c.m. frame of reference. However, the collision cross section is a function of the relative energy in the collision. The freestream viscosity and mean free path are evaluated based on N_2 species using the VHS collision model with $T_{ref} = 2880$ K, $d_{ref} = 3.08 \times 10^{-10}$ m and $\bar{s} = 0.73$. Energy exchange between the translational and internal modes is modeled by the Larsen–Borgnakke statistical model[20] with rotational and vibrational relaxation numbers of 5 and 50, respectively.

Continuum Method

The Navier–Stokes solver consists of an axisymmetric three-temperature, five-species implicit code. The set of equations solved consists of global mass, species mass, axial and radial momentum, global energy, rotational, and vibrational energy conservation equations. The code uses Roe's upwind scheme for the spatial inviscid fluxes, achieving second-order accuracy with the MUSCL scheme. The time integration is accomplished using an implicit lower–upper symmetric Gauss–Seidel (LU–SGS) scheme. This scheme was chosen because it only requires the inversion of a diagonal matrix at each point in the flowfield. With the large number of equations being solved, this is an attractive feature. A complete description of this method and modeling is presented in Ref. 16.

To account for the effects of the Knudsen layer that develops on the surfaces in low-density flows, slip boundary conditions are used. The modeling employed accounts for velocity, temperature, and species concentration slip effects. A more detailed description of the slip boundary conditions used is given in Ref. 17.

As shown in some previous comparisons between solutions using the DSMC method and the Navier–Stokes equations,[17] a meaningful comparison can be achieved, provided the physical model employed by the two methods are matched as closely as possible. By doing this, the effects of using different physical models can be reduced, and the differences between the two solution procedures can be better observed. Thus, the chemical kinetic model[18] and relaxation rates employed in the DSMC method are also employed in the continuum calculations.

Different grids were used for the four test cases investigated. For each flow condition a couple of grid refinements were conducted to ensure accurate capturing of the shock and flowfield features. The cell Reynolds numbers based on local speed of sound near the surface were nominally 2.

Freestream and Wall Conditions

The freestream conditions considered are those experienced by a typical space vehicle for an altitude range of 105–75 km during Earth entry, and are listed in Table 1. The entry velocity considered is 7 km/s. The geometry selected for the present calculations is the same as the Mars Pathfinder probe.[21] It is a 70-deg blunt cone with a 2.65 m diameter and an afterbody as shown in Fig. 1. The freestream parameters along with selected results are summarized in Table 2. The free-

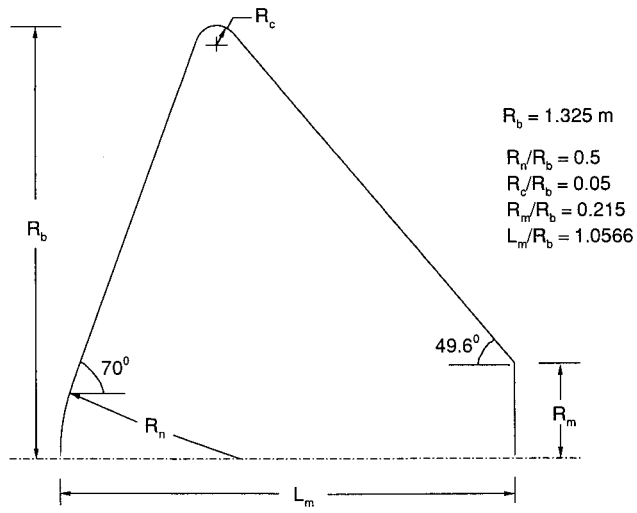

Fig. 1 Blunt body configuration.

Table 1 Freestream conditions[a]

Case	Altitude, km	ρ_∞, 10^{-6} kg/m^3	T_∞, K	$\mathcal{M}$, g/mol	X_{O_2}	X_{N_2}	X_O	λ_∞, mm
1	105	0.232	211.10	27.84	0.1528	0.7818	0.0654	245.9
2	95	1.396	189.10	28.61	0.1972	0.7868	0.0160	40.91
3	85	7.955	180.65	28.96	0.2372	0.7628	0.00	7.189
4	75	41.900	200.00	28.96	0.2372	0.7628	0.00	1.397

[a]T_w = 1000 K, V_∞ = 7.0 km/s.

Table 2 Selected results and flow parameters

Case	Altitude, km	Kn_∞	M_∞	S_∞	Re_∞	Re_2	$C_{H_{stag}}$	C_D
1	105	0.0928	23.47	19.71	311	9.79	0.655	1.78
2	95	0.0154	25.21	21.12	2,031	58.48	0.310	1.66
3	85	0.0027	25.98	21.74	11,970	331.6	0.103	1.65
4	75	0.0005	24.69	20.66	58,530	1746	0.035	1.67

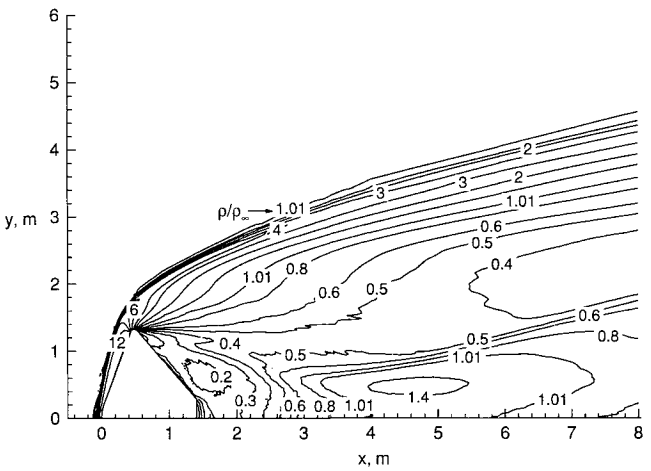

Fig. 2 Selected contours of nondimensional density (altitude = 75 km, Kn_∞ = 0.0005).

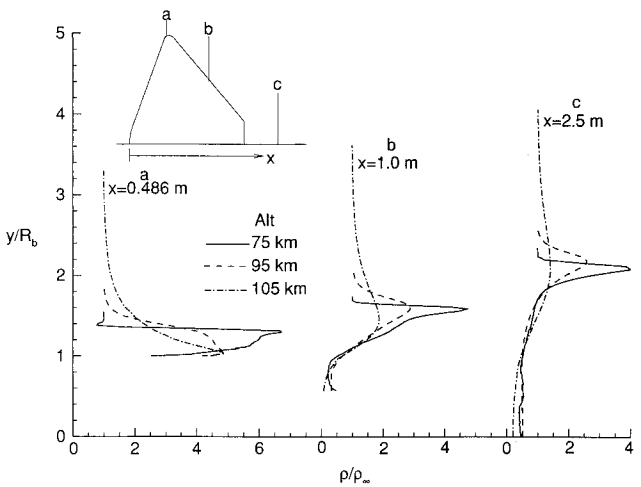

Fig. 3 Rarefaction effects on wake density.

stream mean free path is based on the VHS model, and it is calculated from the relation[14]:

$$\lambda_\infty = \frac{(T_\infty/T_{ref})^\omega}{[\sqrt{2}n_\infty\sigma_{ref}(2-\omega)^\omega\Gamma(2-\omega)]} \quad (1)$$

$$\omega = \bar{s} - 1/2 \quad (2)$$

The gas-surface interaction is assumed to be diffuse with full thermal accommodation to a constant surface temperature of 1000 K. Also, the wall is treated as a noncatalytic surface. The chemical kinetics model[18] contained five species (O_2, N_2, O, N, and NO) with 34 chemical reactions.

Results and Discussion

The DSMC and Navier–Stokes calculations were performed for the 70-deg blunt cone for a range of altitudes during Earth entry. Results of DSMC calculations are discussed first demonstrating the impact of rarefaction on flowfield and surface quantities. Then comparisons between DSMC and Navier–Stokes calculations are discussed for two (85 and 105 km) altitudes.

Rarefaction Effects on Wake Structure

For the 105–75 km altitude range considered, the freestream Knudsen number based on the base diameter varies from 0.0928 to 0.0005 (local wake Knudsen numbers are much larger, ranging from 220 to 0.5), and the forebody and wake

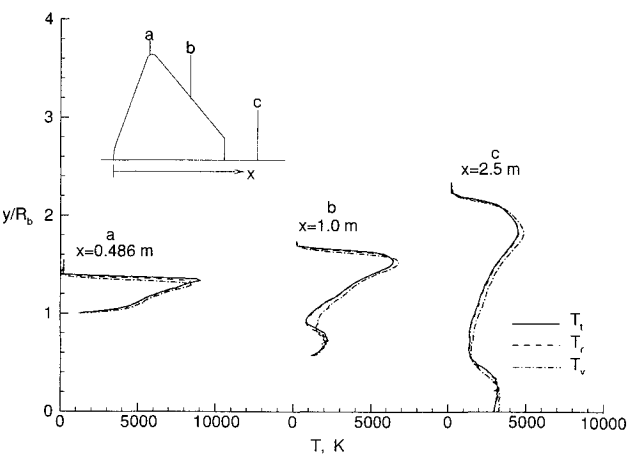

Fig. 4 Wake temperatures profiles (altitude = 75 km, Kn_∞ = 0.0005).

flows features change significantly. A stable vortex is evident at 75 and 85 km altitudes, but not at the higher altitudes considered. At 75 km, the density contours (Fig. 2) show evidence of a weak wake shock, a feature not evident at higher altitudes. Figures 3–6 present radial profiles for several flowfield quantities at three axial locations: location a (x = 0.486 m) corresponds to the maximum radial dimension of the probe, location b (x = 1.0 m) is on the afterbody, and location c (x = 2.5 m) is in the near wake. The impact of rarefaction on the radial density profiles may be observed in Fig. 3 where

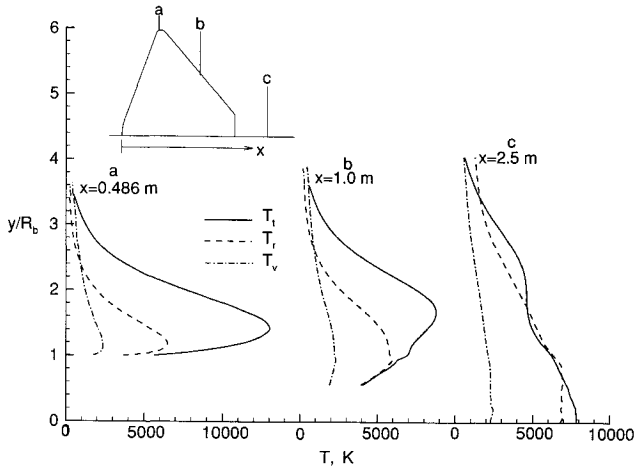

Fig. 5 Wake temperatures profiles (altitude = 105 km, Kn_∞ = 0.0928).

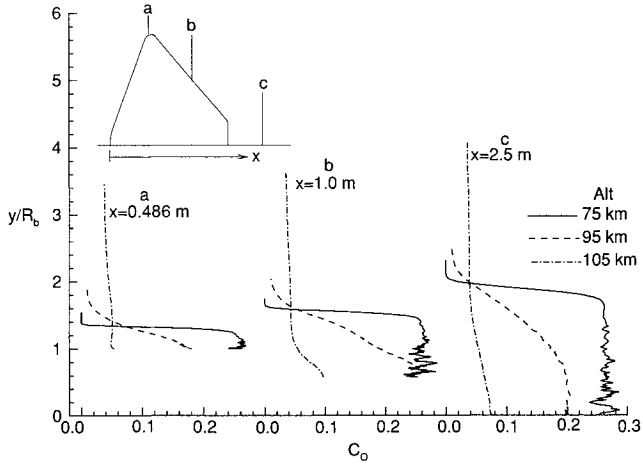

Fig. 6 Atomic oxygen mass fraction profiles.

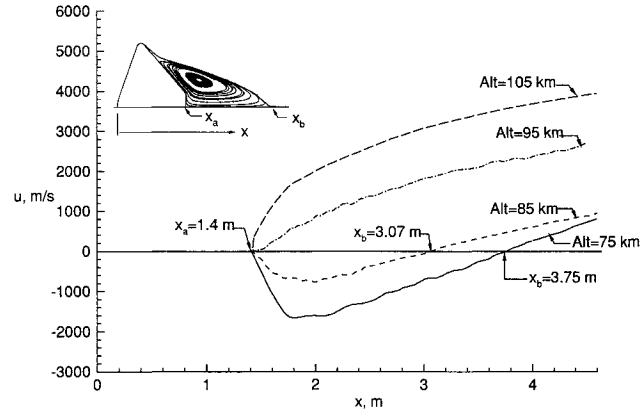

Fig. 7 Rarefaction effects on wake stagnation point.

the most significant differences occur in the bow shock and within the shear layer as the rarefaction increases. The near wake region is shadowed by the forebody ($y/R_B < 1.0$) and the density is generally less than 50% of the freestream value at locations b and c.

Comparison of translational, rotational, and vibrational temperatures in the wake is shown in Figs. 4 and 5 for 75 km and 105 km altitudes, respectively. It can be seen from these figures that the flow is near thermal equilibrium for a 75 km altitude (Fig. 4). For a 105 km altitude, however, the flow is in a highly thermal-nonequilibrium state. Also, for 105 km, the temperature jump is significant along the afterbody surface (Fig. 5).

Along the forebody, essentially all molecular oxygen and about half of the molecular nitrogen is dissociated before reaching the body surface at altitudes of 75 and 85 km. The mass fractions of atomic oxygen in the wake are shown in Fig. 6. It can be seen from Fig. 6 that the mass fraction of atomic oxygen remains almost constant (C_0 = 0.26) behind the bow-shock for 75 km altitude. The concentration of atomic oxygen decreases significantly (Fig. 6) with increasing altitude. A similar behavior is observed for atomic nitrogen.[22]

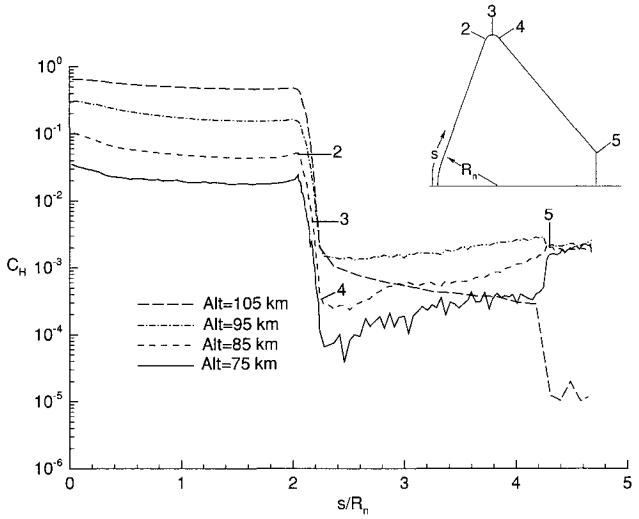

Fig. 8 Effect of rarefaction on heat transfer coefficient.

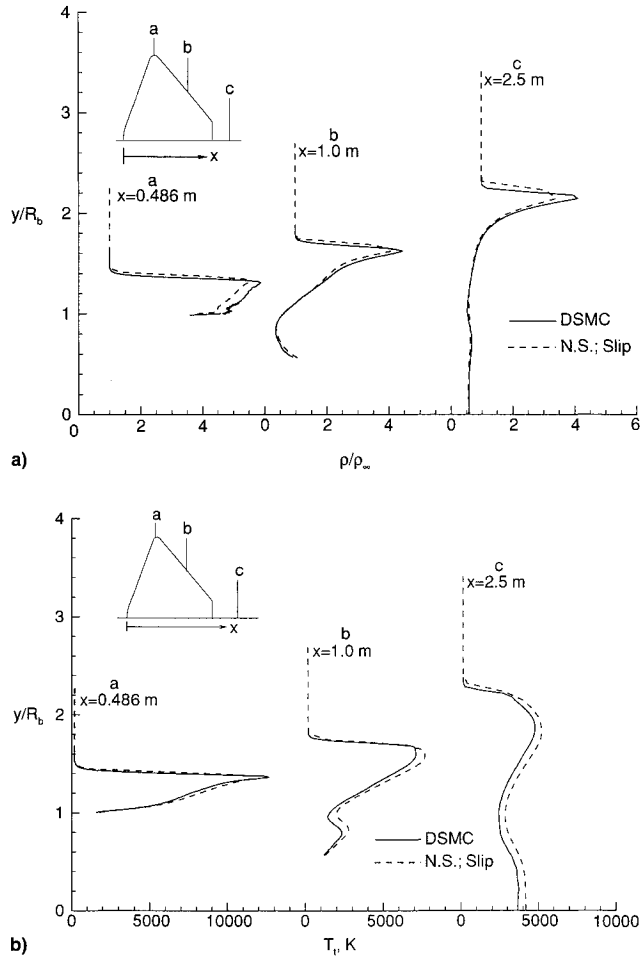

a)

b)

Fig. 9 Comparisons of DSMC and Navier–Stokes results (altitude = 85 km, Kn_∞ = 0.0027): a) nondimensional density profiles and b) translational temperature profiles.

The wake stagnation point for axisymmetric flows is the location along the wake symmetry axis where the velocity is zero. The effect of rarefaction on the location of the wake stagnation point is shown in Fig. 7. It can be seen from Fig. 7 that the wake stagnation point moves toward the rear stagnation point as altitude increases from 75 to 85 km and coincides with the rear stagnation point for altitudes of 95 and 105 km. It also implies that there exists a large stable vortex for 75 and 85 km altitudes, whereas the flow is attached for 95 and 105 km altitudes.

Rarefaction Effects on Surface Quantities

The effects of rarefaction on heat transfer coefficient are presented in Fig. 8. The results are shown as a function of nondimensional distance (s/R_n) along the surface measured from the forebody stagnation point. Expansion of the flow about the corner reduces the afterbody surface coefficients orders of magnitude compared to their forebody values. The forebody heat transfer is very sensitive to rarefaction (Fig. 8) as is the skin-friction.[22] However, the forebody pressure is rather insensitive to rarefaction (Ref. 22). Along the afterbody the heat transfer coefficient experiences a significant decrease in value for the 105 km altitude, suggesting that the near wake flow is becoming free molecular.

Comparison of DSMC and Navier–Stokes Results

DSMC and Navier–Stokes calculations were performed for all four altitudes listed in Table 1. Comparisons of results for density and temperature in the wake are shown in Figs. 9 and 10 for altitudes of 85 and 105 km, respectively. The radial density and translational temperature profiles (Figs. 9a and 9b) show good agreement between DSMC and Navier–Stokes results for the 85 km altitude case. The agreement becomes less and less favorable with increasing altitude. For 105 km altitude there is a significant difference between DSMC and Navier–Stokes results (Figs. 10a and 10b), clearly indicating that Navier–Stokes equations are inadequate to model such

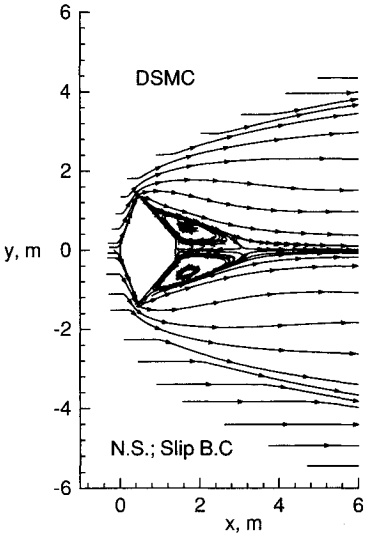

Fig. 11 Comparison of DSMC and Navier–Stokes streamlines (altitude = 85 km, Kn_∞ = 0.0027).

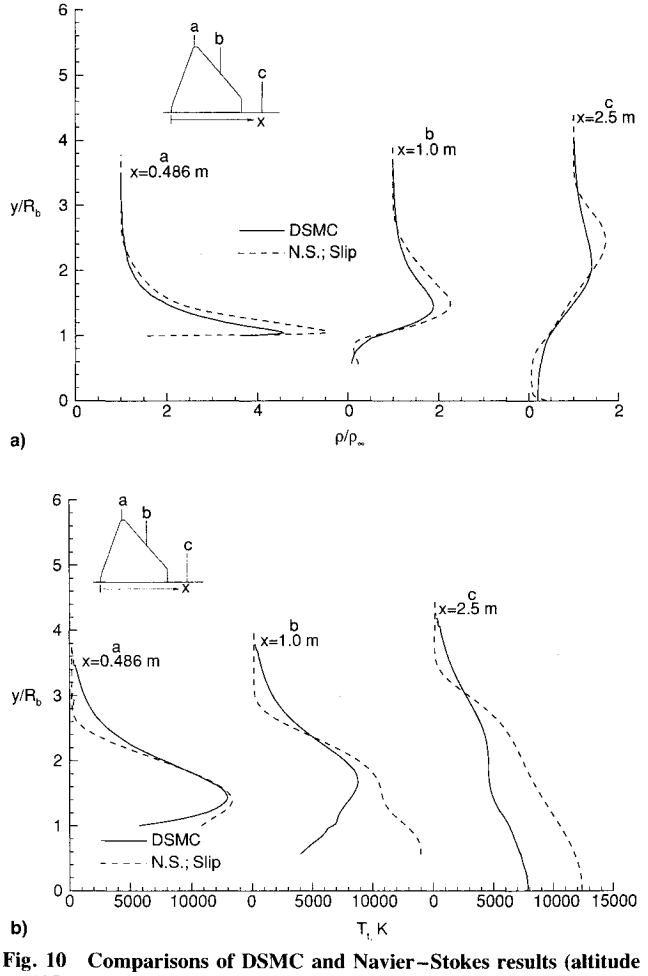

Fig. 10 Comparisons of DSMC and Navier–Stokes results (altitude = 105 km, Kn_∞ = 0.0928): a) nondimensional density profiles and b) translational temperature profiles.

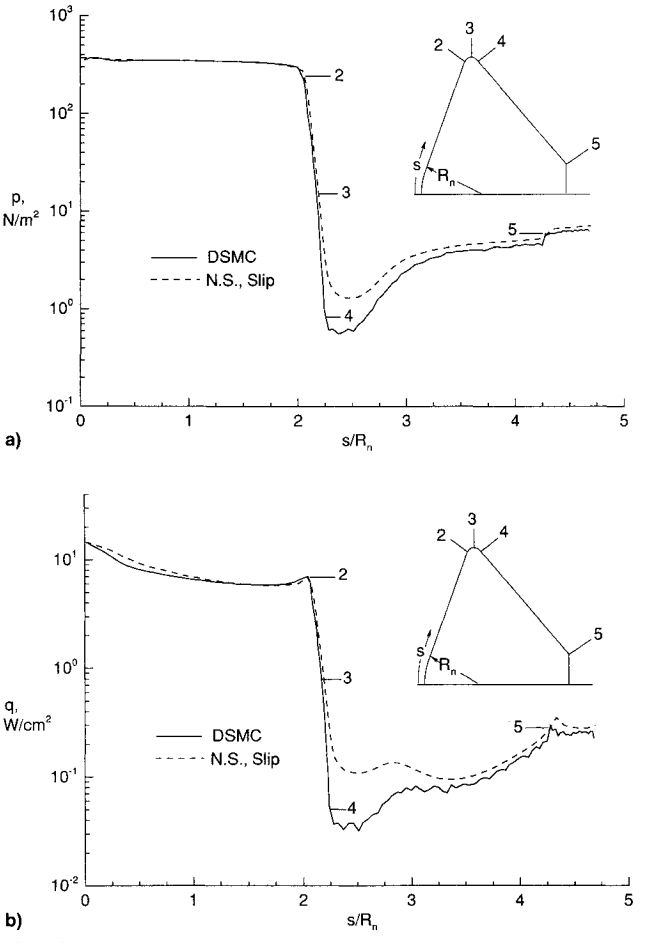

Fig. 12 Comparisons of DSMC and Navier–Stokes surface results (altitude = 85 km, Kn_∞ = 0.0027): a) surface pressure and b) surface heating rate.

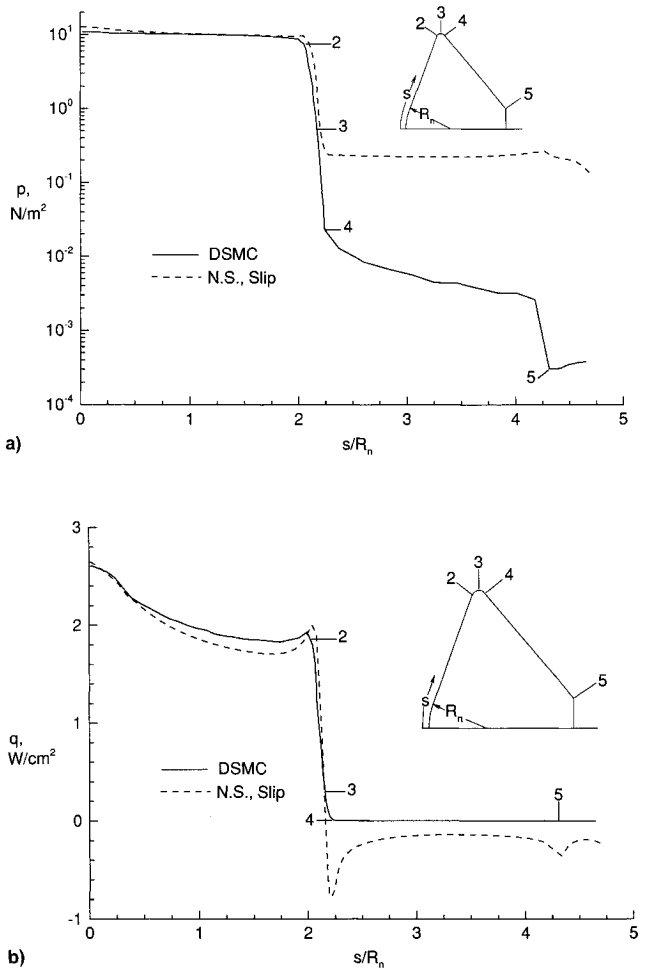

Fig. 13 Comparisons of DSMC and Navier–Stokes surface results (altitude = 105 km, Kn_∞ = 0.0928): a) surface pressure and b) surface heating rate.

rarefied flow conditions. As shown in Ref. 22, the Navier–Stokes calculations predict lower mass fractions of atomic oxygen and atomic nitrogen in the wake region compared to the DSMC results. There is also a significant difference in the mass fractions of atomic oxygen and atomic nitrogen predicted by DSMC and Navier–Stokes calculations for all other altitudes. Both DSMC and Navier–Stokes calculations predict a steady vortex in the wake region for 75 and 85 km altitudes as shown in Fig. 11 for the 85-km case.

DSMC and Navier–Stokes (with slip boundary conditions) results for surface pressure and heating are shown in Figs. 12 and 13 for 85 and 105 km altitudes, respectively. These surface quantities are shown in semilog scale as a function of nondimensional distance (s/R_n) along the surface measured from the stagnation point in order to give a better perspective of the magnitudes along the afterbody surface. For the 85-km case, Navier–Stokes and DSMC results are in good agreement for both heating rate and pressure (Fig. 12) along the forebody. Along the afterbody, however, Navier–Stokes results are somewhat higher than DSMC results (Fig. 12). For the 105 km altitude (Fig. 13), Navier–Stokes and DSMC surface results are still in reasonable agreement along the forebody, but differ significantly along the afterbody. With the very rarefied wake flow at 105 km, the continuum model no longer can simulate such flows accurately.

Concluding Remarks

DSMC and Navier–Stokes (with slip boundary conditions) axisymmetric calculations of hypersonic rarefied flows about a 70-deg blunt cone have been performed. The flow conditions considered are those experienced by a space vehicle for an altitude range of 105–75 km during Earth entry. The entry velocity considered is 7 km/s. Particular emphasis is given to the effects of rarefaction on the wake structure and the surface quantities.

A stable vortex exists for 75 and 85 km, whereas the flow remains attached to the body surface for 95 and 105 km altitudes. A weak wake shock is evident at 75 km, but not at higher altitudes. The surface heat transfer is very sensitive to the rarefaction effects. The surface quantities along the forebody surface calculated by Navier–Stokes calculations are in reasonable agreement with DSMC results for all altitudes. Along the afterbody surface results differ significantly. These differences increase with increasing altitude, clearly showing that Navier–Stokes equations are inadequate to simulate such rarefied wake flows.

References

[1]*America at the Threshold*, Rept. of the Synthesis Group on America's Space Exploration Initiative, Superintendent of Documents, U.S. Government Printing Office, Washington, DC, 1991, p. 59.

[2]Moss, J. N., and Price, J. M., "Direct Simulations of AFE Forebody and Wake Flow with Thermal Radiation," *Rarefied Gas Dynamics*, edited by E. P. Muntz, D. P. Weaver, and D. H. Campbell, Vol. 118, Progress in Astronautics and Aeronautics, AIAA, Washington, DC, 1989, pp. 413–431.

[3]Gnoffo, P. A., Price, J. M., and Braun, R. D., "On the Computation of Near Wake, Aerobrake Flowfields," *Journal of Spacecraft and Rockets*, Vol. 29, No. 2, 1992, pp. 182–189.

[4]Dogra, V. K., Moss, J. N., Wilmoth, R. G., and Price, J. M., "Hypersonic Rarefied Flow Past Spheres Including Wake Structure," *Journal of Spacecraft and Rockets*, Vol. 31, No. 5, 1994, pp. 713–718.

[5]Brewer, E. B., "Hypersonic Rarefied Wake Characterization," NASA TP-3327, Jan. 1993.

[6]Lumpkin, F. E., Boyd, I. D., and Venkatapathy, E., "Comparison of Continuum and Particle Simulations of Expanding Rarefied Flows," AIAA Paper 93-0728, Jan. 1993.

[7]Dogra, V. K., Moss, J. N., Wilmoth, R. G., and Price, J. M., "DSMC Simulations of Hypersonic Low-Density Flow About an ASTV Including Wake Structure," *Rarefied Gas Dynamics*, edited by B. D. Shizgal and D. P. Weaver, Vol. 160, Progress in Astronautics and Aeronautics, AIAA, Washington, DC, 1992, pp. 199–208.

[8]Dogra, V. K., Moss, J. N., and Price, J. M., "Near Wake Structure for a Generic Configuration Aeroassisted Space Transfer Vehicles," *Journal of Spacecraft and Rockets*, Vol. 31, No. 6, 1994, pp. 953–959.

[9]Moss, J. N., Mitcheltree, R. A., Dogra, V. K., and Wilmoth, R. G., "Hypersonic Blunt Body Wake Computations Using DSMC and Navier-Stokes Solvers," AIAA Paper 93-2807, July 1993.

[10]Wilmoth, R. G., Mitcheltree, R. A., Moss, J. N., and Dogra, V. K., "Zonally-Decoupled DSMC Solutions of Hypersonic Blunt Body Wake Flows," AIAA Paper 93-2808, July 1993.

[11]Moss, J. N., Dogra, V. K., and Wilmoth, R. G., "DSMC Simulations of Mach 20 Nitrogen Flows About a 70-Deg Blunted Cone and Its Wake," NASA TM 107762, Aug. 1993.

[12]Dogra, V. K., Moss, J. N., Wilmoth, R. G., Taylor, J. C., and Hassan, H. A., "Effects of Chemistry on Blunt Body Wake Structure," AIAA Paper 94-0352, Jan. 1994.

[13]Bird, G. A., *Molecular Gas Dynamics*, Clarendon, Oxford, England, UK, 1976.

[14]Bird, G. A., "Monte Carlo Simulation in Engineering Context," *Rarefied Gas Dynamics*, Vol. 74, Pt. I, edited by S. S. Fisher, AIAA, New York, 1981.

[15]Bird, G. A., "Direct Simulation of Gas Flows at the Molecular Level," *Communications in Applied Numerical Method*, Vol. 4, No. 2, 1988, pp. 165–172.

[16]Olynick, D. R., and Hassan, H. A., "New Two-Temperature Dissociation Model for Reacting Flows," *Journal of Thermophysics and Heat Transfer*, Vol. 7, No. 4, 1993, pp. 687–696.

[17]Olynick, D. R., Taylor, J. C., and Hassan, H. A., "Comparisons Between DSMC and the Navier-Stokes Equations for Reentry Flows," AIAA Paper 93-2810, July 1993.

[18]Moss, J. N., and Bird, G. A., "Direct Simulations of Transitional

Flow for Hypersonic Re-Entry Conditions," *Thermal Design of Aeroassisted Orbital Transfer Vehicles*, edited by H. F. Nelson, Vol. 96, Progress in Astronautics and Aeronautics, AIAA, New York, 1985, pp. 113–139.

[19]Dogra, V. K., Moss, J. N., and Simmonds, A. L., "Direct Simulations of Aerothermal Loads for an Aeroassist Flight Experiment Vehicle," AIAA Paper 87-1546, June 1987.

[20]Borgnakke, C., and Larsen, P. S., "Statistical Collision Model for Monte Carlo Simulation of Polyatomic Gas Mixtures," *Journal of Computational Physics*, Vol. 18, No. 4, 1975, pp. 405–420.

[21]Tauber, M., Henline, W., Chargin, M., Papadopoulos, P., Chen, Y., Yang, L., and Hamm, K., "Mesur Probe Aerobrake Preliminary Design Study," AIAA Paper 92-2952, July 1992.

[22]Dogra, V. K., Moss, J. N., Wilmoth, R. G., Taylor, J. C., and Hassan, H. A., "Rarefaction Effects on Blunt Body Wake Structure for Earth Entry Conditions," AIAA Paper 94-2016, June 1994.